Inelastic Proton Scattering at 40 MeV†

TANNIE STOVALL* AND NORTON M. HINTZ
School of Physics, University of Minnesota, Minneapolis, Minnesota
(Received 13 March 1964)

Inelastic proton scattering has been studied using 40-MeV protons as the projectile particle. Energy spectra of protons scattered from Li^7, C^{12}, Al^{27}, Ca^{40}, Fe^{54}, Fe^{56}, Ni^{58}, Ni^{60}, Cu^{63}, Pb^{206}, Pb^{207}, and Pb^{208} have been taken. Angular distributions have been taken on the strongly excited states of C^{12}, Mg^{24}, Fe^{54}, Fe^{56}, Ni^{58}, Ni^{60}, and Pb^{208}. The Blair phase rule is found to apply moderately well when a pronounced diffraction structure exists in the angular distributions. It is found that the McCarthy-Kromminga rule for the determination of parities of nuclear states from the small angle behavior of the angular distributions has limited validity. The $B(EL)$'s obtained from proton inelastic scattering measurements, using a distorted-wave Born approximation analysis, agree fairly well with the values obtained by electromagnetic methods.

I. INTRODUCTION

In recent years a number of inelastic scattering experiments have been performed in which the final nucleus is left in a state of low excitation and for which the bombarding energy is greater than 15 or 20 MeV.[1–9] These reactions go predominately via a direct interaction process. For particles which are strongly absorbed by the nucleus one finds angular distributions of scattered particles that exhibit a regular diffraction pattern. The diffraction pattern is particularly pronounced if the Q of the reaction is small. Moreover, the more opaque the nucleus to the incident particle the sharper is the observed diffraction structure.

In comparing reactions of the type (p,p'), (e,e'), (d,d'), and (α,α') both similarities and differences are observed. It is found that states strongly excited in inelastic scattering via the nuclear force are also, in general, strongly excited by Coulomb excitation. Thus states strongly excited in inelastic scattering reactions are usually collective[10] states corresponding to a single 2^L pole disturbance of the nuclear surface. These collective states are to be contrasted with the single-particle states preferentially excited in pickup, stripping, and knock-on reactions of the type (p,n). The collective nuclear states in some cases seem to be excited in inelastic scattering with the same relative probability regardless of the kind of incident particle or energy of the incident particle[11]; in other cases the same states are not excited with the same relative probability for different bombarding particles.[12]

Some of the inelastic scattering experiments previously published were made with good resolution, less than 0.5%. The measurements presented here were taken with slightly worse resolution, ~1%. Measurements with higher resolutions are forthcoming, but it was decided that because of the scarcity of proton inelastic scattering measurements, the present results should be published. In this paper we report on some measurements of inelastic proton scattering at 40 MeV. Section II of this paper contains the experimental details. In Sec. III some elementary theoretical considerations are discussed. In Sec. IV the data and calculations

TABLE I. Data for targets used in this experiment.

Target	Area density (ρx) mg/cm²	Isotopic purity
Li^7	34	97.57
C	70	natural
Mg	27	natural
Al^{27}	8.1	natural
Ca^{40}	40	natural
Fe^{54}	48.2	94.68
Fe^{56}	48.6	99.7
Ni^{58}	65.5	99.6
Ni^{60}	79.5	98.51
Cu^{63}	55.6	99.85
Pb^{206}	7.80	99.8
Pb^{207}	8.05	82.57
Pb^{208}	7.45	99.75

† Work supported in part by the U. S. Atomic Energy Commission.
* Present address: National Bureau of Standards, Washington, D. C.
[1] Kazuhisa Matsuda, Nucl. Phys. **33**, 536 (1962).
[2] B. L. Cohen and A. G. Rubin, Phys. Rev. **111**, 1568 (1958); G. Schrank, E. K. Warburton, and W. W. Daehnick, *ibid.* **127**, 2159 (1962); D. W. Devins, H. H. Forster, and G. G. Gigas, Nucl. Phys. **35**, C17 (1962); N. M. Hintz, C. D. Kavaloski, L. L. Lee, Jr., and T. Stovall, *Rutherford Jubilee International Conference, Manchester, England, 1961*, edited by J. B. Birks (Academic Press Inc., New York, 1961), p. 509.
[3] R. S. Slobodrian, Phys. Rev. **125**, 1003 (1962); B. L. Cohen and R. E. Price, *ibid.* **123**, 283 (1961); J. L. Yntema and B. Zeidman, *ibid.* **114**, 815 (1959).
[4] R. H. Crannel, H. Helm, R. Kendall, H. Oeser, and M. Yearian, Phys. Rev. **123**, 923 (1961).
[5] J. Bellicard and P. Barreau, Nucl. Phys. **36**, 476 (1962).
[6] S. Saudinos, Ph.D. thesis, de L'Universite de Paris, 1962 (unpublished).
[7] R. Beurtey, P. Catillon, R. Chaminade, M. Crut, H. Faraggi, A. Popineau, J. Saudinos, and J. Thirion, Compt. Rend. **252**, 1756 (1961).
[8] H. W. Broek, T. H. Braid, J. L. Yntema, and B. Zeidman, Phys. Rev. **126**, 1514 (1962).
[9] D. K. McDaniels, J. S. Blair, S. W. Chen, and G. W. Farwell, Nucl. Phys. **17**, 614 and 641 (1960); M. Crut, D. R. Sweetman, and N. S. Wall, *ibid.* **17**, 635 (1960); H. J. Watters, Phys. Rev. **103**, 1763 (1956); J. L. Yntema, B. Zeidman, and B. J. Raz, *ibid.* **117**, 801 (1960).
[10] B. L. Cohen, Phys. Rev. **116**, 426 (1959).
[11] H. W. Kendall, *Proceedings of the Conference on Direct Interactions and Nuclear Reaction Mechanisms*, edited by E. Clemental and C. Villi (Gordon and Breach Publishers, Inc., New York, 1963), p. 711.
[12] M. Barloutaud, K. Chaminade, H. Faraggi, D. Goretta, and B. G. Harvey (private communication).

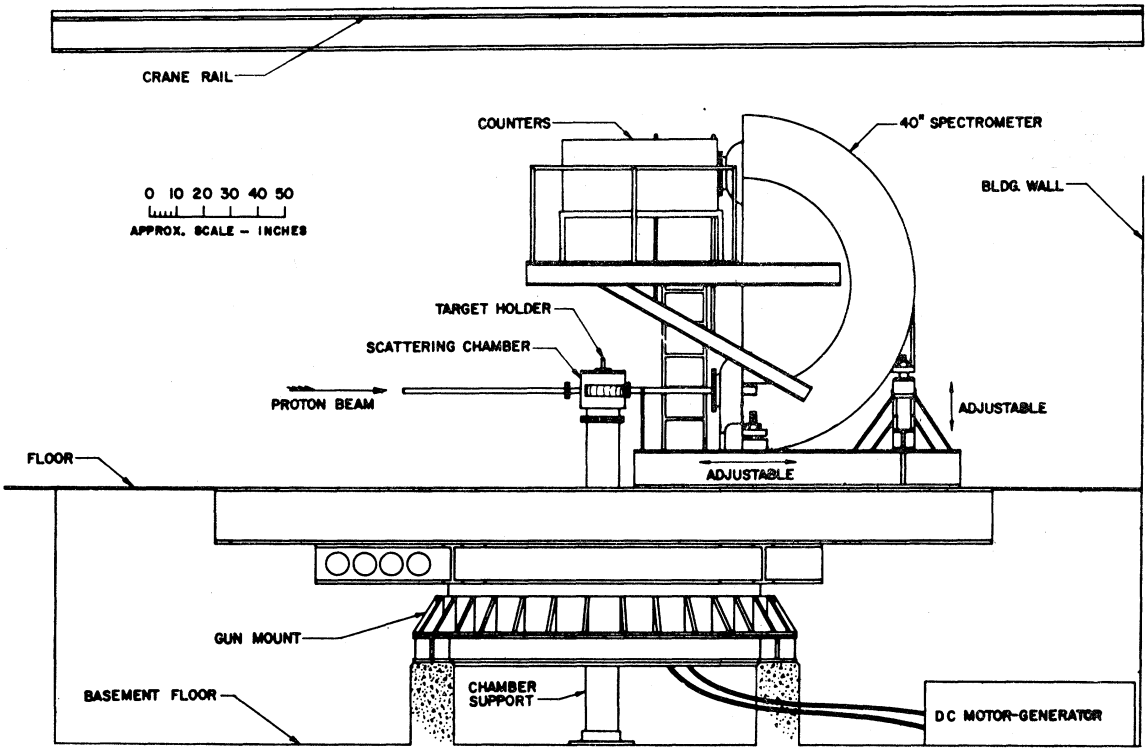

FIG. 1. Plan view of scattering chamber and magnetic spectrometer.

are presented, and Sec. V contains comments and conclusions.

II. APPARATUS AND EXPERIMENTAL PROCEDURE

A. Beam Geometry

A beam of protons average energy 39.8 MeV was extracted from the third tank of the Minnesota linac and bent 7° into a 12-in.-diam Mylar-windowed scattering chamber at the magnetic spectrometer position. The beam was focused at the target with a three-element magnetic quadrupole lens, 35 ft from the scattering chamber. The estimated beam energy spread at the target is 0.75%. The beam spot at the collimators was oval shaped, about $\frac{1}{4}$ in. in the vertical plane and about $\frac{1}{2}$ in. in the horizontal plane. The horizontal extension was due mostly to beam energy spread. The beam was collimated with a complement of 2 defining and 2 antiscattering collimators. The 2 defining collimators, $\frac{1}{4}$ in. in diameter, were situated 10 and 43 in., respectively, from the target and the antiscattering collimators were situated 6 and 27.5 in., respectively, from the target.

B. Targets

The targets were self-supporting foils. The targets were isotopically enriched except for those of carbon, magnesium, and calcium. The isotopically enriched targets were secured from the Isotope Division of the Oak Ridge National Laboratory. Relevant information on the targets is given in Table I.

C. Beam Monitoring System

The beam was collected in a small Faraday cup, situated inside the scattering chamber about 4 in. behind the target. The Faraday cup was about 50 MeV thick for protons and had a circular aperture, $\frac{3}{4}$-in. i.d. The geometry of the Faraday cup allows one to observe particles that scatter through an angle greater than 7°. The charge collected on the Faraday cup was measured with a beam current integrator described elsewhere.[13] The measurement of the incident charge is not expected to have an absolute accuracy of better than 10 or 20%, owing to the small size of the Faraday cup. However, the relative accuracy is expected to be much better. The Faraday cup is immersed in a 40-g magnetic field which prevents the slower moving electrons from escaping the Faraday cup. Absolute cross sections were determined by calibrating the entire system using known elastic cross sections.

D. Detection System

The scattered beam was magnetically analyzed with a 180-deg sector, 40-in. radius. double focusing astigmatic magnetic spectrometer (Fig. 1). The distance along the optic axis of the spectrometer from the magnet pole pieces to the source was 30 in. The entrance aperture to the spectrometer was defined by a rectangular

[13] Minnesota Linac Progress Reports, 1960 and 1961 (unpublished).

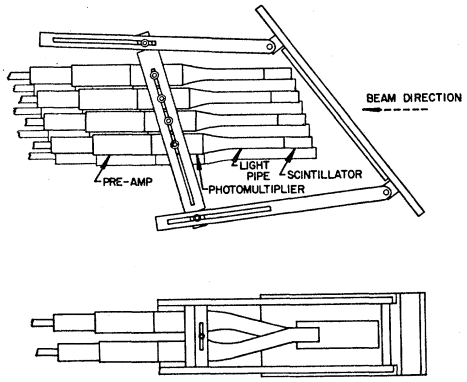

FIG. 2. Sketch of 10-channel detector used in spectrometer focal plane.

baffle 5.38 in. in the radial direction by 0.7 in. in the axial direction, located at the entrance edge of the magnetic pole pieces. With this geometry the ultimate resolution obtainable with the spectrometer as calculated from second-order aberration theory is approximately 0.2% for a point source. The scattered particles were detected in the focal plane of the magnetic spectrometer with a 10-channel scintillation counter detector (Fig. 2). Each unit of the 10-channel detector was 0.75 in. high in the radial (vertical) plane of the spectrometer and with about 0.025 in. of dead region between every two adjacent detectors. The scintillation detectors were made of Pilot B plastic scintillator. They were 1 in. wide in the axial direction and $\frac{1}{2}$ in. deep, just sufficient to stop a 40-MeV proton.

Each unit of the 10-detector array then viewed an energy interval equal to 1% of the average beam energy in the detector [see Eq. (2) below]. The 10-counter array was thus capable of viewing a 10% energy interval.

Protons elastically scattered from carbon were focused in various positions in the counter array to measure the spectrometer transmission. The variation

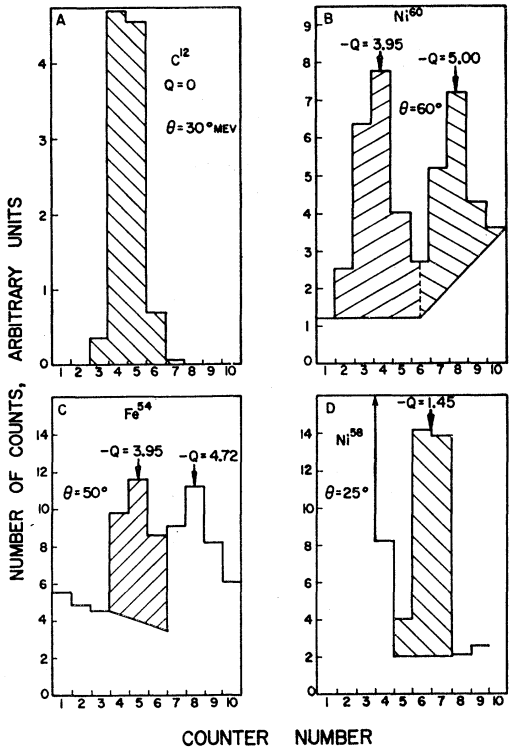

FIG. 3. Typical spectra taken with 10-channel detector. Shaded areas show data reduction procedures. Figure A is an energy spectrum of protons elastically scattered from carbon. This was the best example of an isolated peak. Figures B and C show cutting procedure for peaks close together. In figure D is a typical 2^+ state sitting on the tail of the ground-state group.

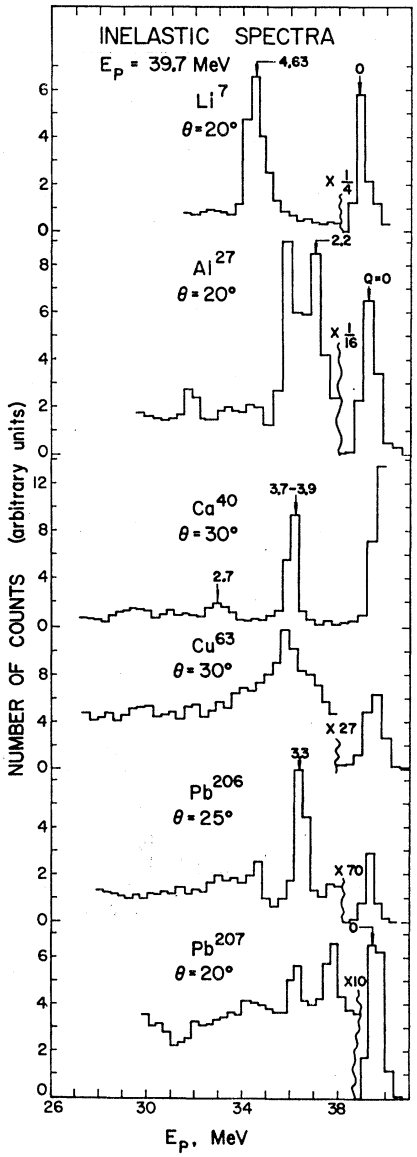

FIG. 4. Energy spectra of 39.8-MeV protons inelastically scattered from Li^7, Al^{27}, Ca^{40}, Cu^{63}, Pb^{206}, and Pb^{207}. Numbers on the figures give Q values of the prominent peaks in MeV.

in efficiency across the array was found to be approximately 5%, and to vary monotonically. This is the same magnitude as the fluctuations of the efficiency which one would expect due to the fact that the peaks sometimes are centered on the dead layer between crystals and sometimes in the center of a crystal.

The signal from each unit of the 10-detector array was fed into a preamplifier[13] and from the preamplifier into a 2-channel pulse-height analyzer.[13] The 2-channel pulse-height analyzers were completely independent of one another with respect to dead time losses. Each individual 2-channel pulse-height analyzer could count any two pulses more than 1-μsec apart. With the typical linac pulse length of 200 μsec and repetition rate of 30 per sec, one could count up to 60 counts per sec, time averaged, in each unit of the 10-channel detector with dead time losses of 1% or less.

At a particular spectrometer magnetic field setting these occur in each counter protons with energy E_0, deuterons with energy $E_0/2$, He^3 ions with energy $4/3E_0$, tritons with energy $E_0/3$, and alpha particles with energy E_0. For values of E_0 of interest in this experiment, the yield of tritons, He^3 ions, and alpha particles in the analyzed beam is quite small compared to the proton yield. The deuteron yield is somewhat larger; however, the two-channel pulse-height analysis is sufficient to distinguish between protons and deutrons.

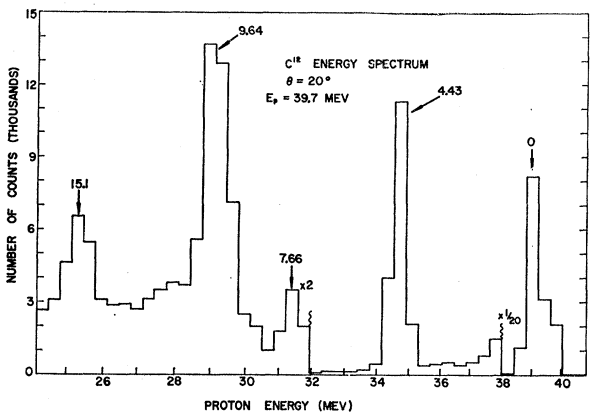

FIG. 5. Energy spectra of 39.7-MeV protons scattered from carbon at 20°. Numbers on figure gives Q values for the prominent peaks in MeV.

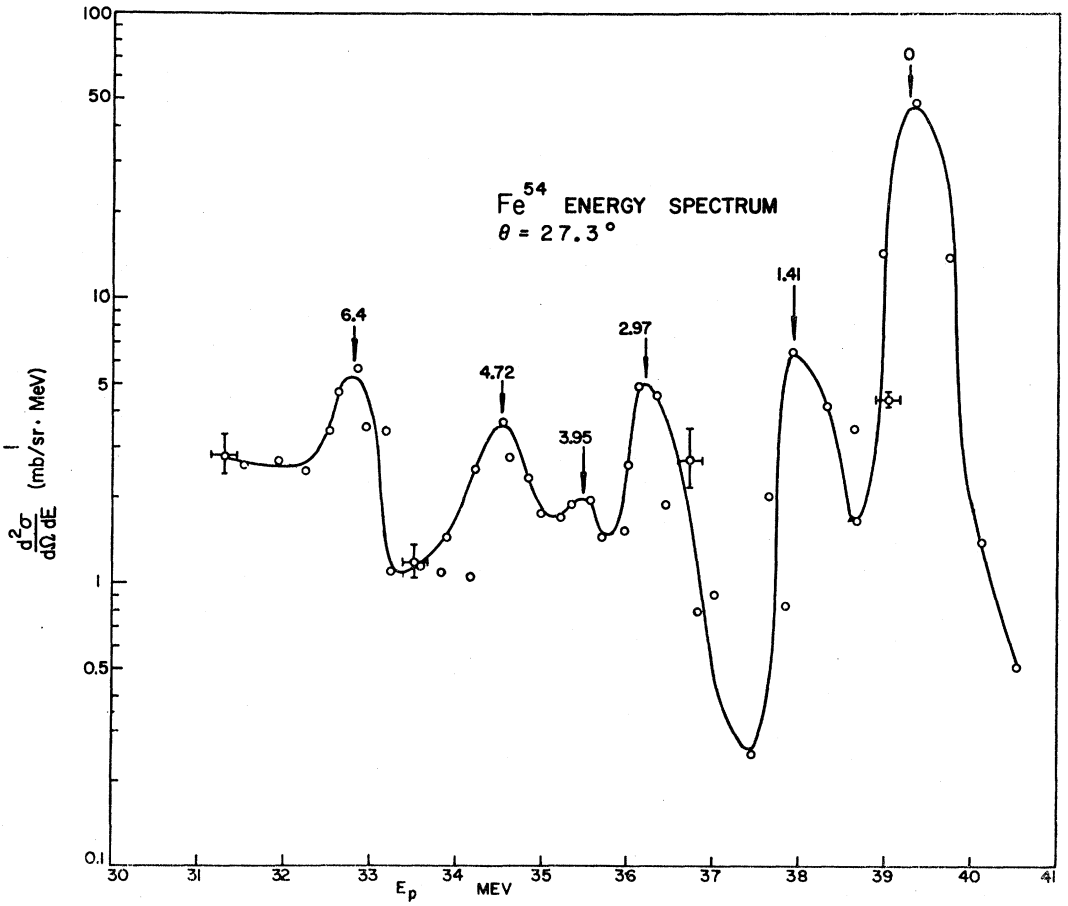

FIG. 6. Distribution ($d^2\sigma/d\Omega dE$) of 39.7-MeV protons scattered from Fe^{54} at 27.3°. Numbers on figure give Q values for prominent peaks in MeV.

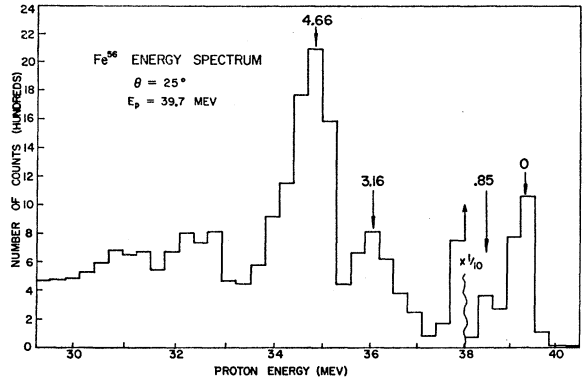

FIG. 7. Energy spectra of 39.7-MeV protons scattered from Fe^{56} at 25°. Numbers on figures give Q values of prominent peaks in MeV.

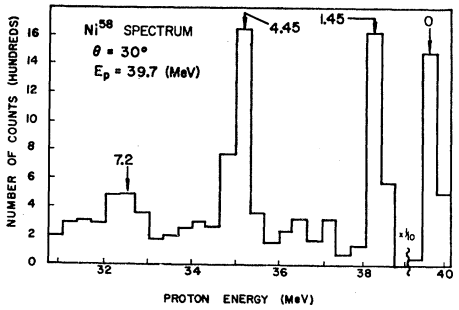

FIG. 8. Energy spectra 39.7-MeV protons scattered from Ni^{58} at 30°. Numbers show Q values for prominent peaks, in MeV.

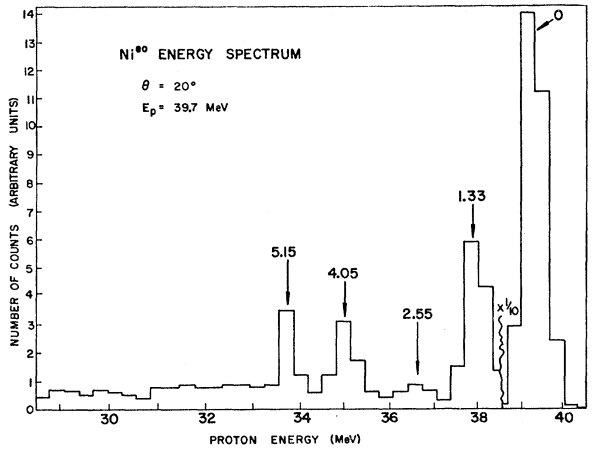

FIG. 9. Energy spectra of 39.7-MeV protons scattered from Ni^{60} at 20°. Numbers show Q values for prominent peaks, in MeV.

E. Background

The counters were shielded from the target and the input collimators with 2 in. of steel, 12 in. of paraffin, and approximately 18 in. of Masonite. With this shielding, the background was negligible at the pulse height of the inelastic protons of interest. Pile up due to the background gave a counting rate of less than 1% of the rate due to protons of energy $\gtrsim 25$ MeV.

F. Data Reduction and Errors

Typical momentum spectra taken with the 10-counter array are shown in Fig. 3 along with typical data extraction procedures. In order to plot complete energy spectra (Figs. 4 through 10) it was necessary to piece together several overlapping spectra taken with the 10-channel detector. The energy scale for the spectra was constructed assuming a linear relation between B^2 and energy and using the spectrometer dispersion equation [Eq. (2)]. The linear relationship was checked using $p-p$ scattering from polyethylene at various angles. The energy points on the spectra have a relative ac-

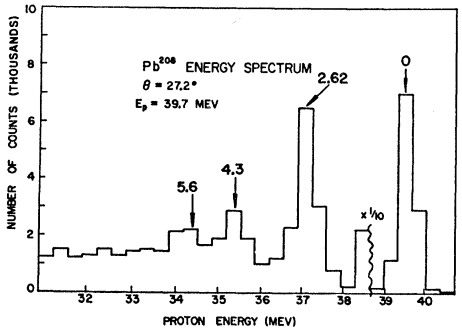

FIG. 10. Energy spectra of 39.7-MeV protons scattered from Pb^{208}. Numbers show Q values for prominent peaks, in MeV.

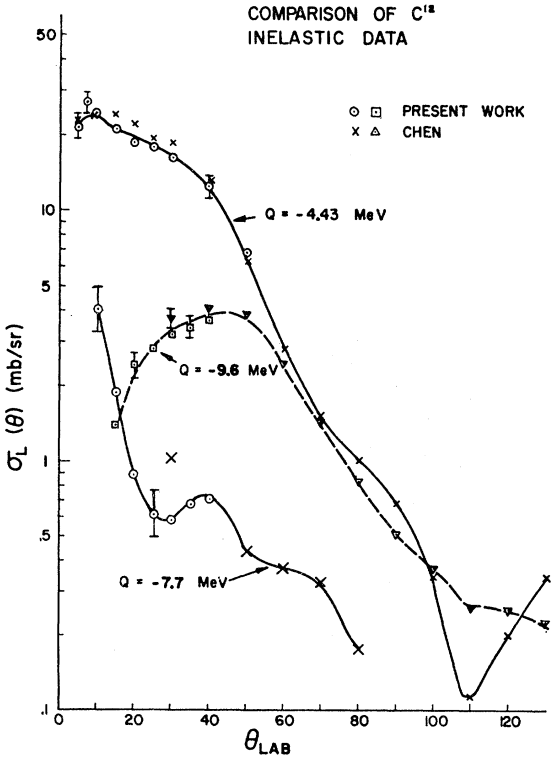

FIG. 11. Angular distribution of protons inelastically scattered from carbon. The large angle points are mostly the work of Chen and Hintz (Ref. 36).

curacy of ±200 keV and an absolute accuracy of ±500 keV.

In order to obtain angular distributions the number of counts in a particular inelastic group must be extracted from the various 10-counter spectra. The uncertainty connected with this operation ranges from 20% for back-angle scattering from well resolved low-lying states to a factor of 3 for small angle scattering

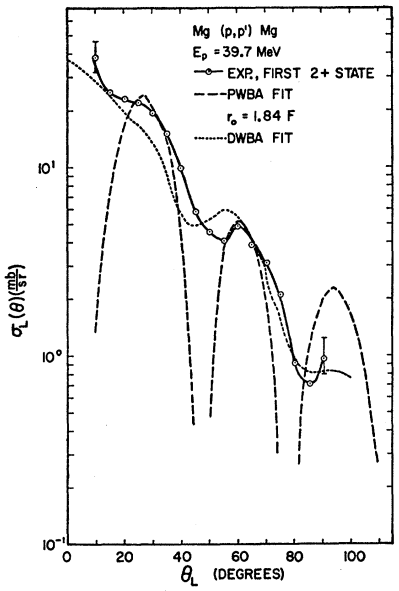

FIG. 12. Angular distribution of protons inelastically scattered from the 2^+ state of Mg^{24}. The dashed line is a PWBA fit to the data and the dotted line is a DWBA fit. The parameters of the optical potential are given in Table IV; the extracted deformation parameter is given in Table III.

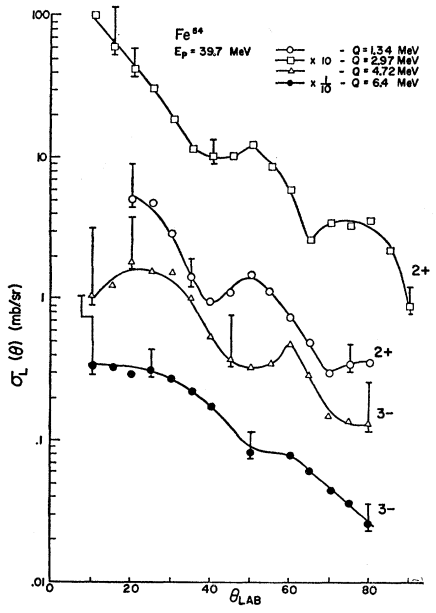

FIG. 13. Angular distributions of strong proton groups inelastically scattered from Fe^{54}.

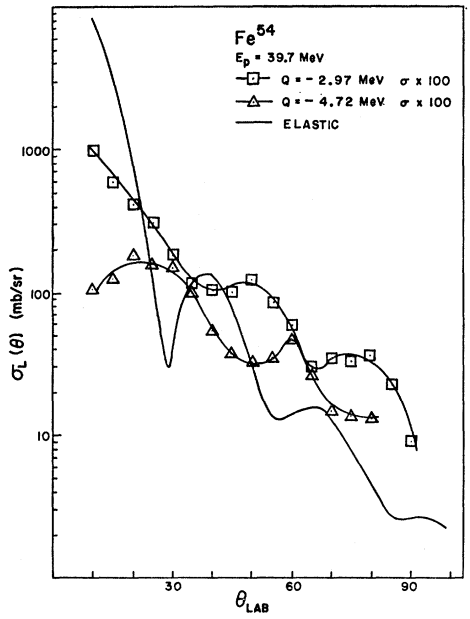

FIG. 14. Angular distributions of protons elastically scattered from Fe^{54} and strong inelastic groups with $-Q=2.97$ and 4.72 MeV.

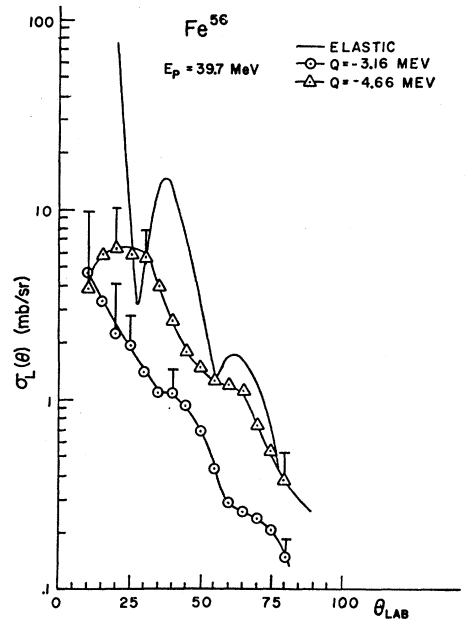

FIG. 15. Angular distributions of strong proton groups scattered from Fe^{56}. The elastic scattering is the work of Brussel and Williams (Ref. 14).

from states standing on a background of unresolved states. Statistical errors and absolute normalization errors for the angular distributions were small compared to errors acquired in reducing the measured 10-channel energy spectra. Error bars on the angular distributions (Figs. 11 through 18) show upper and lower limits of uncertainty due to the peak integrating procedure. Absolute cross sections were obtained by measuring the

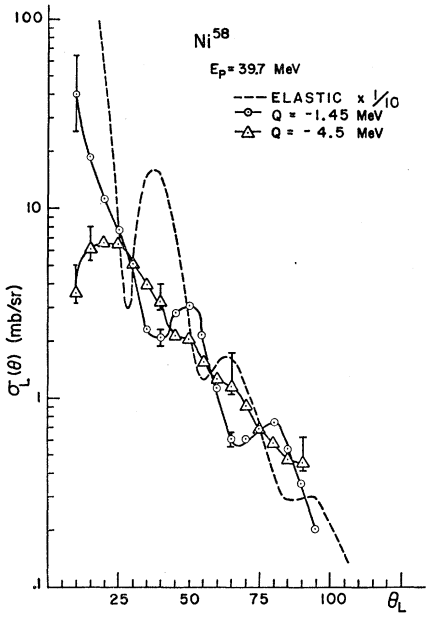

FIG. 16. Angular distribution of strong proton groups scattered from Ni^{58}. The elastic scattering is the work of Brussel and Williams (Ref. 14).

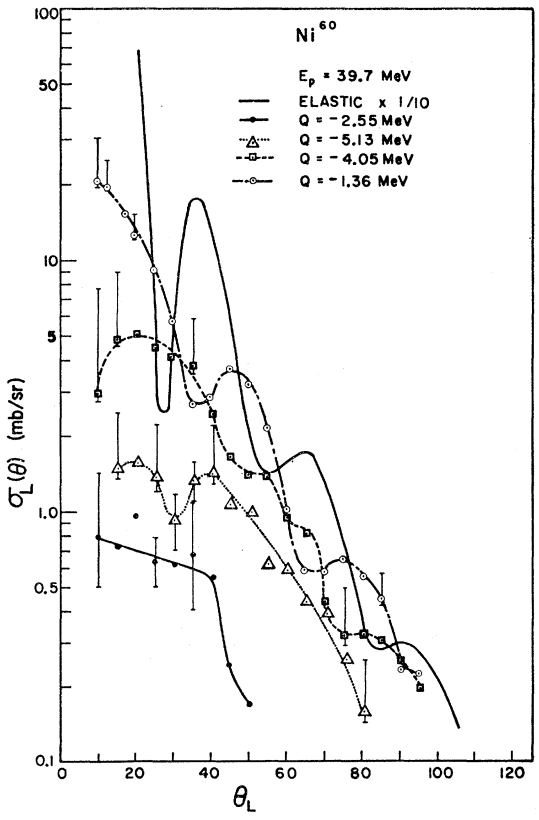

FIG. 17. Angular distribution of strong proton groups scattered from Ni^{60}. The elastic scattering is the work of Brussel and Williams (Ref. 14).

TABLE II. Observed strongly excited states of nuclei.

Isotope	Q(MeV) (p,p')	Probable corresponding level from reference
Li^{7}	4.3 ±0.2	4.63
C^{12}	4.43±0.1	4.43
	7.66±0.1	7.66
	9.63[a]	9.63
	15.11±0.2	15.11
Mg^{24}	1.37±0.15	1.37
Al^{27}	1.92±0.2	2.21
	2.88±0.2	2.98
Ca^{40}	4.02±0.2	3.90
	7.18±0.2	
Fe^{54}	1.34±0.2	1.41
	2.97±0.2	2.97
	3.95±0.2	
	4.72±0.2	
	6.40±0.2	
Fe^{56}	3.16±0.2	
	4.66±0.2	
Ni^{58}	1.45[a]	1.45
	3.33±0.2	
	4.5[a]	4.5
	7.19±0.2	
Ni^{60}	1.36±0.1	1.33
	2.55±0.2	
	3.23±0.2	
	4.05±0.2	4.04
	5.13±0.2	
	7.08±0.2	
Pb^{206}	3.32±0.2	
	4.88±0.2	
Pb^{207}	2.56±0.2	
	4.68±0.2	
Pb^{208}	2.62±0.1	2.62
	4.35±0.2	
	5.62±0.2	
	7.40±0.2	

[a] Calibration state.

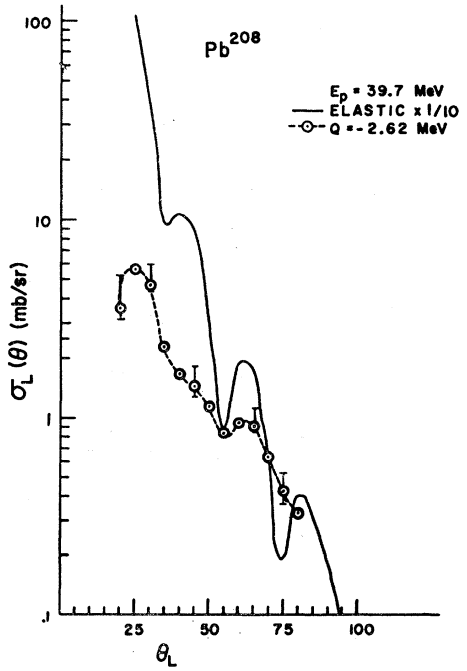

FIG. 18. Angular distribution of 39.7-MeV protons inelastically ($Q=-2.62$ MeV) scattered from Pb^{208}. The elastic scattering is the work of N. M. Hintz (Ref. 15).

ratio of elastic to inelastic scattering at various angles and using previously measured elastic scattering data at 40 MeV.[14,15] This method was used for all absolute inelastic scattering measurements except for Mg^{24} where no measurements of the elastic scattering were available. The elastic scattering cross section at selected angles for Mg^{24} was estimated by an extrapolation from the 40-MeV scattering data of Li^{7}, C^{12}, Al^{27}, and Fe^{54}.[14,15]

G. Q Values

Q values for the prominent peaks are given in Table II. The errors in the Q values listed are mostly due to the uncertainty in locating the position of the peak in the 10-channel spectra and to fluctuations in the beam energy.

The Q values were determined by situating the elastic peak in the center of the counter array and noting the

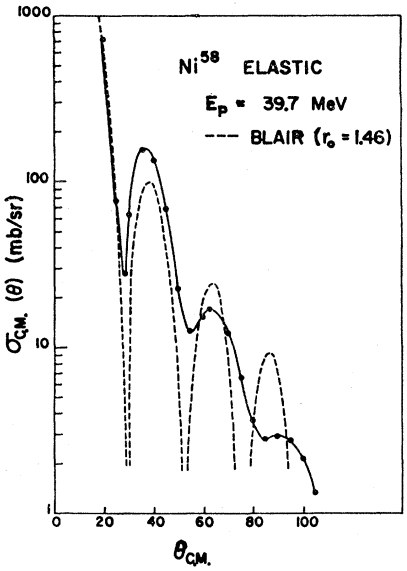

FIG. 19. Blair-Drozdov fit to the elastic proton scattering from Ni^{58}. The parameters used to obtain this fit are given in Table III.

spectrometer magnetic field strength required. Then the energy of the elastically scattered group was calculated using the linac beam design energy and the kinematic relation which relates bombarding energy, scattering energy, and scattering angle. Energies were corrected for energy loss in the target, exit window of the scattering chamber and entrance window of the magnetic spectrometer. The Q value for the various peaks was then determined from the relation

$$Q=\frac{A+1}{A}E-\frac{A-1}{A}E_0-\frac{2}{A}(EE_0)^{1/2}\cos\theta, \qquad (1)$$

where E_0 is the bombarding energy at the center of the target, E is the lab energy of the inelastic groups, and θ is the laboratory scattering angle. This procedure was checked against known Q values. In general, the elastic peak and the inelastic peaks appeared in slightly different positions of the counter array. Corrections for this were made using the dispersion relation for the spectrometer,[16]

$$\Delta x/R=2(\Delta E/E_0), \qquad (2)$$

where Δx is the displacement in the focal plane, meas-

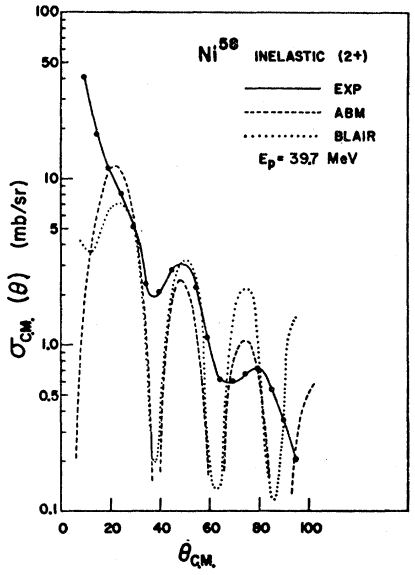

FIG. 20. Blair-Drozdov and PWBA fits to the inelastic reaction $Ni^{58}(p,p')Ni^{58*}$, $Q=-1.45$ MeV. The parameters used to obtain these fits are given in Table III.

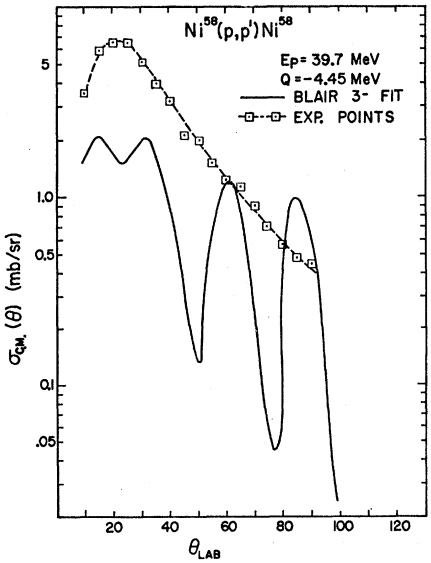

FIG. 21. Blair-Drozdov fit to the inelastic scattering from Ni^{58}, $Q=-4.45$ MeV. The parameter used to obtain the fit are given in Table III.

[14] M. K. Brussel and J. H. Williams, Phys. Rev. **114**, 525 (1959).
[15] Norton M. Hintz, Minnesota Linac Progress Report, p. 31, March 1958 (unpublished).
[16] D. L. Judd, Rev. Sci. Instr. **21**, 213 (1950).

TABLE III. Summary of results from this and other experiments.

Element	Fit	State	$-Q$ (MeV)	r_0 (F)	C_L (MeV)	β_L	θ norm lab	$G=\frac{B(EL)}{B_{sp}(EL)}$	Reference
				Inelastic proton scattering					
Mg^{24}	PWBA	2^+	1.37	1.84					Present work
Ni^{58}	PWBA	2^+	1.45	1.42					Present work
C^{12}	Blair	2^+	4.43	1.46	420	0.162	64°	0.378	Present work
Mg	Blair	2^+	1.37	1.46	31.6	0.329	60°	6.2	Present work
Fe^{54}	Blair	2^+	1.34	1.46	324	0.102	50°	2.81	Present work
Fe^{54}	Blair	2^+	2.97	1.46	880	0.092	50°	2.29	Present work
Fe^{54}	Blair	3^-	4.72	1.46	2300	0.0787	60°	1.63	Present work
Fe^{56}	Blair	2^+	3.16	1.46	1600	0.0685	50°	1.27	Present work
Fe^{56}	Blair	3^-	4.66	1.46	1920	0.0927	60°	2.38	Present work
Ni^{58}	Blair	2^+	1.45	1.46	166	0.148	50°	6.9	Present work
Ni^{58}	Blair	3^-	4.5	1.46	1000	0.125	60°	4.9	Present work
Ni^{60}	Blair	2^+	1.36	1.46	158	0.144	50°	6.5	Present work
Ni^{60}	Blair	3^-	4.05	1.46	1250	0.11	60°	3.8	Present work
Pb^{208}	Blair	3^-	2.62	1.46	4550	0.045	39.6°	5.58	Present work
Mg^{24}	DWBA	2^+	1.37		15.2	0.475		13	Present work
Fe^{54}	DWBA	2^+	1.34		83.4	0.17		8.4	Present work
Fe^{54}	DWBA	2^+	2.97		185	0.17		8.4	Present work
Fe^{54}	DWBA	3^-	4.72		1150	0.12		4.0	Present work
Fe^{54}	DWBA	3^-	6.4		775	0.17		8.6	Present work
Fe^{56}	DWBA	2^+	3.16		467	0.13		4.6	Present work
Fe^{56}	DWBA	3^-	4.66		308	0.23		14.6	Present work
Ni^{58}	DWBA	2^+	1.45		90.6	0.20		12.5	Present work
Ni^{58}	DWBA	3^-	4.5		390	0.20		12.9	Present work
Ni^{60}	DWBA	2^+	1.36		64.4	0.23		16.6	Present work
Ni^{60}	DWBA	3^-			1100	0.09		2.6	Present work
		4^+	2.55		2340	0.07		1.65	Present work
Ni^{60}	DWBA	3^-	4.05		438	0.18		10.4	Present work
Ni^{60}	DWBA	2^+			705	0.14		6.2	Present work
		4^+	5.13		1910	0.11		4.1	Present work
Pb^{208}	DWBA	3^-	2.62		468	0.14		54.0	Present work
				Inelastic electron scattering					
C^{12}		2^+	4.43		69.3	0.4		2.3	a
Mg^{24}		2^+	1.37		13.3	0.508		9	a
Fe^{54}		2^+	1.4		64	0.234		9	b
Fe^{54}		2^+	2.9		486	0.122		4	b
Fe^{54}		3^-	4.85		1140	0.122		4	b
Fe^{54}		3^-	6.4		1230	0.135		5	b
Fe^{56}		3^-	3.1		9740	0.0334		3	b
Fe^{56}		3^-	4.45		600	0.161		7.4	b
Ni^{58}		2^+	1.45		80.0	0.212		14	c
Ni^{58}		3^-	4.5		390	0.201		13	c
Ni^{60}		2^+	1.33		61	0.235		17	c
Ni^{60}		3^-	4.05		284	0.223		16	c
Ni^{60}		4^+	2.5		2140	0.087		3.62	c
Ni^{60}		4^+	5.1		1600	0.12		4.95	c
Pb^{208}		3^-	2.6		793	0.107		31	c
				Inelastic alpha scattering					
C^{12}	Blair	2^+	4.43	2.22	142	0.28	28°	1.13	d, e
Mg^{24}	Blair	2^+	1.37	2.05	60	0.24	28°	3.3	f
Fe^{54}	Blair	2^+	1.41	1.68	352	0.10	21°	2.7	g
Fe^{54}	Blair	4^+	2.47	1.68	12 000	0.03	21°	0.26	g
Fe^{54}	Blair	2^+	2.9	1.68	895	0.09	21°	2.19	g
Fe^{54}	Blair	4^+	3.68	1.68	10 400	0.04	21°	0.47	g
Fe^{54}	Blair	3^-	6.15	1.68	8600	0.05	24°	0.69	g
Fe^{56}	Blair	3^-	3.07	1.68	5300	0.045	25.5°	1.02	h
Fe^{56}	Blair	3^-	4.37	1.68	2100	0.085	25.5°	2.02	h
Ni^{58}	Blair	2^+	1.45	1.68	232	0.13	21°	5.3	h
Ni^{58}	Blair	3^-	4.5	1.38	1820	0.093	27°	2.78	h
Mg^{24}	DWBA	2^+	1.37		43.7	0.28		4.5	i
Ni^{60}	DWBA	2^+	1.33		103	0.18		10.1	i
Ni^{60}	DWBA	3^-	4.50		804	0.14		6.3	i
Ni^{60}	DWBA	4^+	5.50		6880	0.06		1.2	i
				Nuclear resonance scattering					
C^{12}		2^+	4.43	1.2	172	0.254		0.91	j
Mg^{24}		2^+	1.37	1.2	57 to 39	0.292 to 0.765		5 to 32.7	k
Ni^{60}		2^+	1.33	1.2	88	0.184		11.8	l

TABLE III (*continued*)

Element	Fit	State	$-Q$ (MeV)	r_0 (F)	C_L (MeV)	β_L	θ norm lab	$G=\frac{B(EL)}{B_{sp}(EL)}$	Reference
					Direct lifetime measurement				
C^{12}		2^+	4.43	1.2	70.5	0.596		2.26	m
					Coulomb excitations				
Mg^{24}		2^+	1.37	1.2	6.6	0.72		30	k, m
Ni^{58}		2^+	1.45	1.2	95.5	0.195		12	m
Ni^{60}		2^+	1.33	1.2	65	0.226		16	m

[a] R. Helm, Phys. Rev. **102**, 1466 (1956).
[b] J. Bellicard and P. Barreau, Nucl. Phys. **36**, 476 (1962).
[c] R. H. Crannel, H. Helm, R. Kendall, H. Oeser, and M. Yearian, Phys. Rev. **123**, 923 (1961).
[d] A. S. Yavin and G. W. Farwell, Nucl. Phys. **12**, 1 (1959).
[e] S. F. Eccles and D. Bodansky, Phys. Rev. **113**, 608 (1959).
[f] D. K. McDaniels, J. S. Blair, S. W. Chen, and G. W. Farwell, Nucl. Phys. **17**, 614 (1960); **17**, 641 (1960).
[g] S. Saudinos, Ph.D. thesis, de L'Universite de Paris, 1962 (unpublished).
[h] R. Beurtey, P. Catillon, R. Chaminade, M. Crut, H. Faraggi, A. Popineau, J. Saudinos, and J. Thirion, Compt. Rend. **252**, 1756 (1961).
[i] E. Rost, Phys. Rev. **128**, 2708 (1962).
[j] F. Ajzenberg-Selove and T. Lauritsen, Nucl. Phys. **11**, 1 (1959).
[k] P. M. Endt and C. Van Der Leun, Nucl. Phys. **34**, 1 (1962).
[l] F. R. Metzger, Phys. Rev. **107**, 983 (1956).
[m] D. S. Andreyov, A. P. Grinberg, K. I. Erökhino, and I. Kh. Lenberg, Nucl. Phys. **19**, 400 (1960).

ured perpendicular to the optic axis, R is the spectrometer radius of curvature, and ΔE is the energy shift from E_0, the energy which corresponds to the optic axis.

III. THEORY

A. Blair-Drozdov Adiabatic Theory

Theoretical studies of the inelastic scattering from various nuclei have been carried out by many authors.[17–23] The plane-wave Born approximation[18] (PWBA) and the Blair-Drozdov sharp cutoff adiabatic theory[17] predict angular distributions resembling Bessel functions with well-defined maxima and minima which have an envelope that does not fall off with increasing scattering angle as fast as is observed experimentally (see Figs. 19–21). The positions of the maxima and minima are fit fairly well with the PWBA and sharp cutoff adiabatic approximation but in addition to the discrepancy in the fall off at back angles, the peak to valley ratios are larger than observed experimentally. A feature of the sharp cutoff, adiabatic theory, which is expected to work fairly well for strongly absorbed particles is the phase rule, first pointed out by Blair. The Blair phase rule states that the diffraction pattern in the angular distribution of elastically scattered particles is out of phase with that of inelastically scattered particles which leave the nucleus in a state of the same parity as the nuclear ground state, and in phase if the ground state and excited states are states of opposite parity.

The Blair-Drozdov model gives the absolute normalization of the angular distributions in terms of a nuclear deformation parameter β_L or a nuclear surface tension parameter C_L depending on whether the nuclear state is described in terms of a rotational collective excitation or a vibration, respectively. The correspondence between the two normalization parameters is

$$\beta_L^2=(2L+1)(E_{ex}/2C_L), \tag{3}$$

where E_{ex} is the nuclear excitation energy. Values of C_L or β_L obtained from normalizing our data to the Blair theory are given in Table III for comparison with those obtained by other methods. No other parameters are available to fit the data in the Blair theory since the cutoff radius is fixed by fitting the elastic scattering.

Finally, implicit in the Blair-Drozdov model is the parity rule of Kromminga and McCarthy (Sec. IIIC), since the expression for excitation of even parity states contains $|J_0|^2$ which does not vanish at the origin, while that for odd parity states contains only Bessel functions of odd order, all of which vanish at the origin.

B. DWBA with Collective Form Factors

The distorted-wave Born approximation (DWBA) theory for inelastic scattering using collective model form factors has been developed by Satchler and his collaborators.[22] We give here a brief discussion of the theory for vibrational states, noting that the final result may be adjusted to rotational states through Eq. (3). The interaction between the nucleus and the projectile proton is represented by an optical model potential $U[R(\theta',\varphi')]$, where to introduce the collective model it

[17] J. S. Blair, Phys. Rev. **115**, 928 (1959); S. E. Drozdov, Zh. Eksperim. i Teor. Fiz. **28**, 736, 734 (1955) [English transl.: Soviet Phys.—JETP **1**, 588, 591 (1955)].
[18] N. Austern, S. T. Butler, and H. McManus, Phys. Rev. **92**, 350 (1953).
[19] J. S. Blair, D. Sharp, and L. Wilets, Phys. Rev. **125**, 1625 (1962).
[20] N. Glendenning, Phys. Rev. **114**, 1297 (1959).
[21] C. Levinson and M. K. Banerjee, Ann. Phys. (N. Y.) **2**, 471 (1957).
[22] R. H. Bassel, G. R. Satchler, R. M. Drisko, and E. Rost, Phys. Rev. **128**, 2693 (1962).
[23] N. Austern, R. M. Drisko, E. Rost, and G. R. Satchler, Phys. Rev. **128**, 733 (1962).

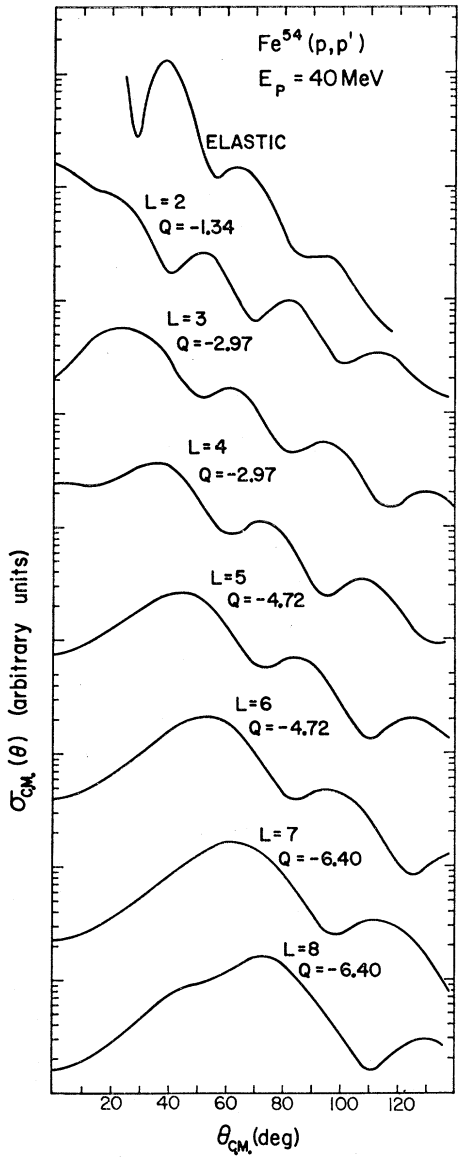

FIG. 22. Typical DWBA predictions for various excited states of Fe^{54}, showing sensitivity of curves to l value. Typical Q values were assumed although the shape of the curves was found to be insensitive to the Q value.

is assumed

$$R(\theta',\varphi')=R_0[1-\sum_{l,m}|\alpha_{lm}|^2/4\pi+\sum_{l,m}\alpha_{lm}Y_l^m(\theta',\varphi')], \quad (4)$$

where θ' and φ' are body-fixed angles. The volume enclosed by this surface is constant to the second order in the nuclear shape parameters, α_{lm}. In Satchler's formulation of the theory it is postulated that the elastic scattering is due to the terms in the optical potential which are zeroth order in the nuclear shape parameters, while the inelastic scattering is due to the real part of higher order terms arising from the optical potential. The inelastic scattering differential cross section is given by

$$\left(\frac{d\sigma}{d\Omega}\right)=\left(\frac{\mu}{2\pi\hbar^2}\right)^2\frac{k_f}{k_i}\sum_{av}|T_{fi}|^2, \quad (5)$$

where μ is the reduced mass and $\hbar k_f$ and $\hbar k_i$ are the final and initial center of mass momenta of the projectile particle, respectively, and

$$T_{fi}=\int[\mathbf{d}r\,\varphi_f^{(-)*}(\mathbf{k}_f,\mathbf{r})\langle f|V_{\rm int}|i\rangle\varphi_i^{(+)}(\mathbf{k}_i,\mathbf{r})], \quad (6)$$

where $\langle f|V_{\rm int}|i\rangle$ is the matrix element of the interaction potential taken between initial and final nuclear states, and $\varphi^{(+)}(\mathbf{k}_f,\mathbf{r})$ and $\varphi^{(-)}(\mathbf{k}_i,\mathbf{r})$ are solutions of the zeroth-order wave equation.

The optical potential $U[R(\theta',\varphi')]$ has many parameters. In principle, all of the optical potential parameters are determined by fitting elastic data. The matrix elements of the α_{lm} are functions of C_L, the surface tension parameters for the vibrational states. With the potential $U(R_0)$ fixed by the elastic data, one normalizes the inelastic scattering by adjusting the surface tension parameter C_L. When $V_{\rm int}$ is assumed proportional to (d/dr) [real, central part of $U(R)$] the inelastic scattering cross section may be written in the form,

$$\frac{d\sigma}{d\Omega}=\frac{2J_{f+1}}{2J_{i+1}}\sum_L|A_L|^2\sigma_L(\theta), \quad (7)$$

where

$$A_L=i^L(R_0V/a)(\hbar\omega_L/2C_L)^{1/2}$$

and $\sigma_l(\theta)$ are reduced differential cross sections which are defined by Satchler *et al.* R_0, V, and A are the optical potential parameters, defined in Eq. (13). $\hbar\omega_L$ is the energy of the state. Thus, the only free parameter in this expression is C_L.

For vibrational states, the α_{lm} are operators which create and annihilate quanta of the nuclear shape oscillations. In the harmonic oscillator approximation, where one expands the potential to terms linear in the deformation one can have only single quanta or single phonon excitations, in the first Born approximation. The first-order Born approximation with terms quadratic in the deformation or second-order Born approximation with terms linear in the deformation gives rise to two phonon excitations.[23] In general, the single-phonon states are more strongly excited than the two-phonon states. It is the single-phonon states which obey the Blair phase rule. The double-phonon states may or may not obey the phase rule.[23]

C. Small Angle Inelastic Scattering, Parity Rule

It has been suggested by Kromminga and McCarthy[24] that one should be able to determine the parity of a nuclear state from the behavior of the small angle in-

[24] I. E. McCarthy and A. J. Kromminga, Phys. Rev. Letters **6**, 62 (1961).

elastic cross section. Kromminga and McCarthy have shown on general grounds that at small angles the nuclear scattering from low-lying states with parities opposite to the ground-state parity have angular distributions that decrease with decreasing angle.

Kromminga and McCarthy have made calculations including distortion effects, which show that the differential inelastic scattering cross sections for protons which leave nuclei in 2^+ states will, in general, increase with decreasing angle at small scattering angles.[25] Experimentally we have found no exception to the above rule. In addition, we observed that all of the 3^- cross sections decrease at small angle. The ability to distinguish positive from negative parity states by the McCarthy-Kromminga rule depends on the excitation energy of the state being small, compared to the bombarding energy. However, typical single-phonon excitation DWBA calculations[26] (Fig. 22) show that the Kromminga-McCarthy rule is only useful for picking out 2^+ single-phonon states, since for all $L \geq 3$ the differential inelastic scattering cross sections decrease with decreasing scattering angle at small angles. On the other hand, the calculations plotted in Fig. 22 show that it is relatively easy to distinguish 2^+, 3^-, and 4^+ states from the position of the first maximum in the inelastic scattering.

D. Electromagnetic Transition Rates

In order to connect our results with those from Coulomb excitation and inelastic electron scattering we give a brief discussion of the quantities measured in electromagnetic excitations. In electromagnetic processes transition rates of a particular multipolarity L are proportional to $B(L)$ where

$$B(L, J_i \rightarrow J_f) = (2J_i+1)^{-1} |\langle J_i \| m(L) \| J_f \rangle|^2, \quad (8)$$

where $m(L)$ is the L-pole moment of the interaction. We shall be concerned with electric interactions only. In the collective model of the nucleus if one assumes that the equilibrium shape of the nucleus is spherical then one obtains a prediction of $B(EL)$ in terms of the nuclear mass and surface tension parameters, β_L and C_L. For small L the values of $B(EL)$ are insensitive to the nuclear charge distribution for several common charge distributions (uniform Gaussian, exponential). For quadrupole vibrational excitations

$$B_{\text{vib}}(E2)/B_{sp}(E2) = 1.0Z^2\hbar\omega_2/C_2, \quad (9)$$

where the single-particle value is

$$B_{sp}(EL) = (1/4\pi)R^{2\lambda}e^2(3/3+L)^2 \quad (10)$$

independent of whether the charge distribution is uniform, Gaussian or exponential. For an octupole disturbance and uniform charge distribution

$$B_{\text{vib}}(E3)/B_{sp}(E3) = 1.43Z^2\hbar\omega_3/C_3 \quad (11)$$

and for a 2^4-pole disturbance for a uniform charge distribution,

$$B_{\text{vib}}(E4)/B_{sp}(E4) = 1.94Z^2\hbar\omega_4/C_4. \quad (12)$$

Experimentally,[27] there is considerable evidence that the low-lying 2^+ states of the nuclei studied in this paper are collective and have gamma-ray transition rates many times greater than the single-particle

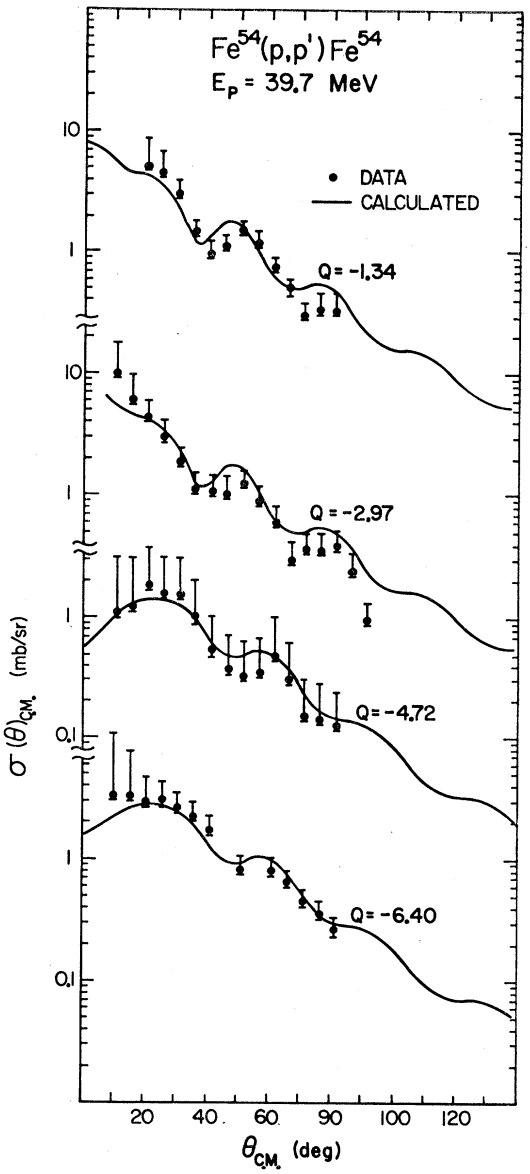

FIG. 23. DWBA fits to the inelastic proton scattering from strongly excited states of Fe^{54}.

[25] A. J. Kromminga and I. E. McCarthy (private communication).

[26] Martin Fricke (private communication).

[27] K. Alder, A. Bohr, J. Huus, B. Mottelson, and A. Winther, Rev. Mod. Phys. 28, 432 (1956).

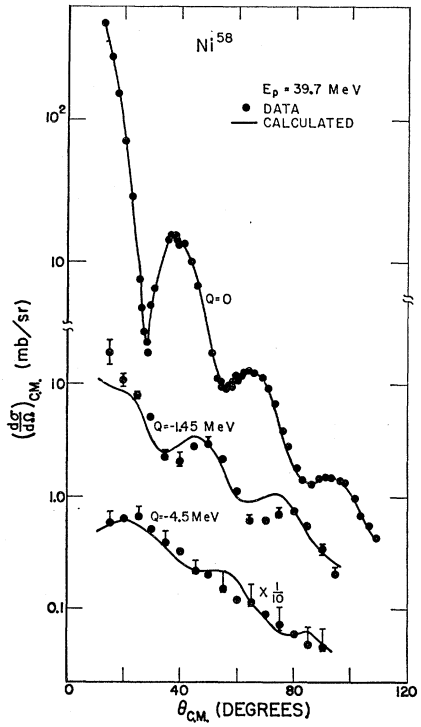

FIG. 24. DWBA fits to the angular distributions of protons scattered from Ni^{58} with $Q=0$, -1.45 and -4.45 MeV.

values. Indeed if one substitutes the values of the deformation parameters extracted from our data one observes that the $B(EL)$ values are greater than the $B_{sp}(EL)$ values.

If the collective model of the nucleus offers a good description of the low-energy electromagnetic properties of the nucleus and if the collective model DWBA is applicable to inelastic proton scattering, then the values of C_L obtained from inelastic scattering should be the same as those extracted from electromagnetic experiments. If the C_L obtained in the two sets of experiments are the same, then one has a powerful tool for determining electromagnetic properties of nuclei from a study of nuclear reactions and vice versa. We shall see in the next section that the evidence indicates that there is a fair coorespondence between the nuclear parameters obtained via the different interactions.

IV. RESULTS

A. General

Survey energy spectra were taken on various elements throughout the periodic table. These energy spectra are given in Figs. 4 through 10. Most of these energy spectra were taken at forward angles. Angular distributions were taken for the strongly excited states in a number of elements (Figs. 11 through 18).

In Table III we have listed values of the nuclear surface tension, C_L, for the various nuclear states studied, assuming that the nuclear states in question are vibrational states. In addition, values of C_L, β_L, and G the ratio $B(EL)/B_{sp}(EL)$ have been extracted from proton, electron, alpha-particle, gamma-ray, direct lifetime, and Coulomb excitation experiments.

The values of B_L and C_L for (p,p') and (α,α') given in Table III are from the Blair-adiabatic approximation and DWBA fits to the data. The values of B_L and C_L derived from the inelastic scattering data will in general depend on the angle at which the theoretical curves are normalized to the experimental curves, especially in the Blair-adiabatic approximation. We have stated this angle when applicable. Generally the theoretical curves for the proton data were normalized at the same diffraction maximum which was used in the analysis of the alpha scattering data. The radius parameter r_0, given in Table III. is either the radius used to estimate $B_{sp}(EL)$ or the radius used to fit the elastic scattering in the Blair-adiabatic approximation. G is either calculated using Eqs. (9), (11), or (12) or by dividing quoted or deduced values of $B(EL)$ by $B_{sp}(EL)$.

The results of the DWBA calculations[26,28] made by Satchler and Fricke at Oak Ridge are plotted in Fig. 12 and Figs. 22–26. The distorting potential used in these

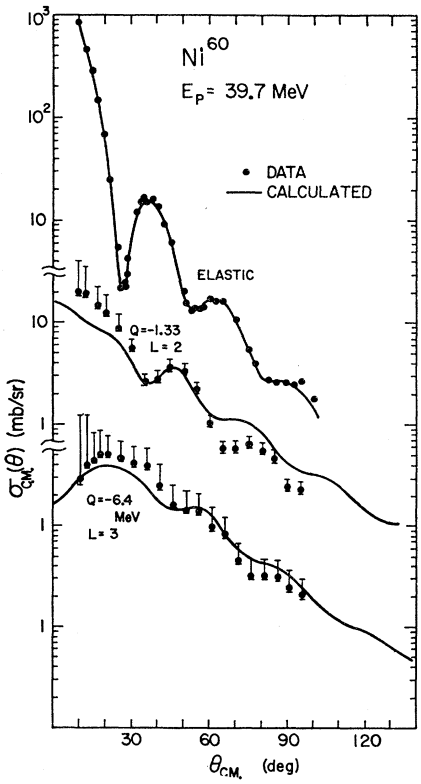

FIG. 25. DWBA fit to the angular distributions of protons scattered from Ni^{60} with $Q=0$, -1.33 and 4.07 MeV.

[28] G. R. Satchler (private communication).

TABLE IV. DWBA optical potential parameters used to obtain fits shown in Figs. 22 through 26 and C_L values given in Table III.

	V	W	W'	W_s	V_s	r_0	r_0'	r_c	A	A'
Fe^{54}	44.8	8.1	0	0	6.51	1.1688	1.4028	1.2	0.7553	0.4405
Fe^{56}	43.5	6.5	0	0	6.37	1.1733	1.4507	1.2	0.7361	0.7582
Ni^{58}	39.6	9.57	0	0	4.5	1.251	1.387	1.2	0.7604	0.2537
Ni^{60}	44.3	7.1	0	0	6.52	1.1648	1.4594	1.2	0.7545	0.5937
Mg^{24}	41.0	42	0	0	6	1.25	1.25	1.25	0.65	0.47
Pb^{208}	51	8.0	0	0	6.6	1.20	1.428	1.2	0.65	0.704

calculations was of the form

$$U(R)=-\frac{V}{e^x+1}-i\left[\frac{w^-}{e^x+1}w'\frac{d}{dx'}\left(\frac{1}{e^{x'}+1}\right)\right]$$
$$-\left(\frac{\hbar}{m_\pi c}\right)^2(V_s+iW_s)\mathbf{l}\cdot\boldsymbol{\sigma}\frac{1}{R}\frac{d}{dR}\left[\frac{1}{e^x+1}\right] \quad (13)$$

plus the Coulomb potential for a uniformly charged sphere of radius r_c, where

$$x=(R-R_0)/a, \qquad R_0=r_0A^{1/3}$$
$$x'=(R-R_0')/a', \qquad R_0'=r_0'A^{1/3}. \quad (14)$$

The parameters for the optical potentials used to fit the data are given in Table IV. In most cases the parameters were obtained from a search which gave the best fit to the elastic angular distributions (Fe^{54}, Fe^{56}, Ni^{58}, Ni^{60}, and Pb^{208}). The optical potential parameters for Mg^{24} were obtained by extrapolating from lower energy data. The Mg^{24} calculations were made with an earlier version of the code which did not contain either a surface absorption term or an imaginary spin orbit term in the distorting potential.

B. Li^7, Al^{27}, Cu^{63}, Ca^{40}, Pb^{206}, Pb^{207}

Energy spectra of Li^7, A^{27}, Cu^{63}, Ca^{40}, Pb^{206}, and Pb^{207} were taken and are shown in Fig. 4. The prominent peaks are tabulated in Table II. Since angular distributions were not measured, no further discussion will be given for these elements.

C. C^{12}

States of C^{12} were observed at 4.4, 7.7, 9.6, and 15.1 MeV. Angular distributions were taken on the 4.4-, 7.7-, and 9.6-MeV states at small angles. These are shown in Fig. 11 along with some earlier measurements by Chen and Hintz.[29]

The small angle behavior of the 9.6-MeV state indicates by the Kromminga-McCarthy rule that it is probably a negative parity state which is consistent with the earlier assignment of 3^-.[30]

The 7.7-MeV state is known to be a 0^+ state[30] and the small angle scattering in the present work is consistent with the plus parity assignment.

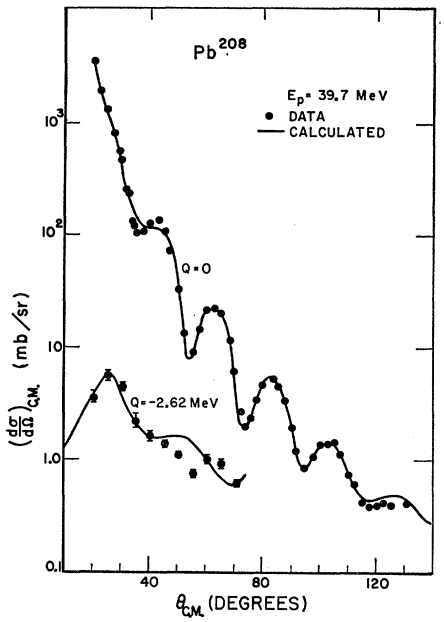

FIG. 26. DWBA fits to the angular distributions of protons scattered from Pb^{208} with $Q=0$, and -2.62 MeV.

The 4.4-MeV state, known to be 2^+, has been examined through inelastic scattering processes with electrons, protons, deuterons, and alpha particles as the projectile.[30] We observe that the angular distribution for 40-MeV proton scattering is a smooth monotonically decreasing function of scattering angle in the range from 10°–105°. For 23-MeV deuterons there is more structure in the angular distribution and for 40-MeV alpha particles one finds a marked diffraction structure. The G values for the 4.4-MeV state of C^{12} are given in Table III as derived from inelastic alpha scattering, inelastic proton scattering, inelastic electron scattering, nuclear resonance scattering, and direct lifetime measurements. The various values agree only within one order of magnitude.

D. Mg^{24}

An angular distribution of protons scattered from the 2^+ state of Mg^{24} at $Q=-1.24$ MeV is measured and is shown in Fig. 12. The dashed line is a PWBA[18] fit to the data, the dotted line is the DWBA fit calculated by Satchler. The quadrupole strength of the 1.37-MeV state of Mg^{24} has been measured in a number of experiments.[31] One finds G values ranging from 3.3 to 32.7. We find values of 6.2 using the Blair approximation and 17.4 from the DWBA. The inelastic proton value of 17.4 agrees fairly well with the inelastic electron measurement of 13.3.[32]

[29] S. W. Chen and N. M. Hintz, *Proceedings of the International Congress on Nuclear Physics, Paris, 1958* (Dunod Cie., Paris, 1958), p. 287.
[30] F. Ajzenberg-Selove and T. Lauritsen, Nucl. Phys. **11**, 1 (1959).
[31] P. M. Endt and C. Van Der Leun, Nucl. Phys. **34**, 1 (1962).
[32] R. Helm, Phys. Rev. **104**, 1466 (1956).

E. Fe^{54}

States of Fe^{54} have been observed at 1.34, 2.97, 3.95, 4.72, and 6.4 MeV (Fig. 6). Angular distributions have been taken on the 1.34-, 2.97-, 4.72-, and 6.4-MeV states (Figs. 13, 14). In electron inelastic scattering[5] at 150 MeV, states have been observed at 1.4, 2.9, 4.1, 4.85, 6.4, and 7.2 MeV. In inelastic alpha-particle[16] scattering at 43 MeV, states have been observed at 1.4, 2.47, 2.8, 3.15, 3.68, 4.14, 4.46, and 6.15 MeV. In the present work the states at 1.34-, 2.97-, 4.72-, and 6.4-MeV excitation of Fe^{54} all have about the same cross sections. The 3.95-MeV state was weaker and therefore difficult to resolve.

$E2$ form factors are found for the 1.4- and 2.9-MeV states of Fe^{54} in the inelastic electron scattering experiments of Bellicard and Barreau.[5] Barloutaud *et al.*[12] also give 2^+ assignments to these states from (α,α') scattering. Our data are consistent with these assignments. The 4.85- and 6.4-MeV levels were given 3^- assignments by Bellicard and Barreau and our data again are consistent in phase and small angle behavior and are well fitted by the $l=3$ DWBA curves (Fig. 23).

The angular distributions of the protons scattered from states of different parity in Fe^{54} are clearly out of phase with each other (Fig. 13). Although the diffraction patterns for the inelastic states in Fe^{54} are definitely in or out of phase with each other they are not either in or out of phase with the elastic scattering (Fig. 14). Consequently, the phase rule is satisfied less rigidly for protons than for alpha particles. This is also observed in the scattering from the nickel isotopes, but less markedly (Figs. 16 and 17).

The ratio of the maximum of the angular distribution to the minimum is considerably smaller than predicted by the Blair-Drozdov theory. Furthermore, the fall-off of the angular distribution with increasing angle is greater than the Blair-Drozdov prediction.

DWBA fits to the data are shown in Fig. 23. The fits were obtained by varying the parameters of the zeroth-order distorting potential until the best possible fit was obtained for the elastic scattering. The best fit to the inelastic scattering was then obtained by adjusting the surface tension parameter C_L. These curves were calculated with pure volume absorption and include Coulomb excitation. Essentially the same curves were obtained using a pure surface absorption potential with only a small change in the C_L value. The values of the surface tension parameter used to fit the data are given in Table III. We note that the G values deduced from inelastic electron scattering and those obtained here are in fair agreement except for the 2^+ state at 2.9 MeV. In electron scattering experiments all the reported states had approximately the same G values except the 1.4-MeV state which had a G value about twice as large as the rest. The G's for the 1.41- and 2.9-MeV states are about equal when protons or alpha-particles are the bombarding projectiles. There does not appear to be a correspondence between the remaining states excited by alpha particles and the states excited by protons and electrons; however, the inelastic alpha-scattering experiments were performed with somewhat better resolution than the inelastic electron and proton experiments, Finally, the DWBA fits confirm the angular momentum assignments given above.

F. Fe^{56}

States of Fe^{56} have been observed at 3.16 and 4.66 MeV (Fig. 7). Angular distributions for the scattering from these states are shown in Fig. 15. With 44-MeV alpha particles Beurtey *et al.*[7] observed states of Fe^{56} at 0.83, 2.04, 2.57, 3.07, 4.37, and 5.04 MeV. The states at 0.83, 3.07, and 4.37 MeV were the strongest. Our data indicates that the 0.83-MeV state is strongly excited, but our resolution was not good enough to separate it. Bellicard and Barreau[5] using 150-MeV electrons have observed states in Fe^{56} at 0.85, 2.7, 3.1, 4.45, and 5.05 MeV.

The 4.66-MeV state observed by us is consistent with a 3^- assignment, which is the spin assignment of the state at 4.45 observed by Bellicard and Barreau and of the 4.37-MeV state observed by Beurtey *et al.*[7] The G values found from the DWBA fit to our proton data agree only to within a factor of 2 with those extracted from the inelastic electron scattering experiments.

In both the inelastic alpha[6] and the inelastic electron experiments[4] the state at $Q=-3.1$ MeV was given an assignment of 3^-. Matsuda[1] has assigned 4^+ to a strong level at 3.12 MeV on the basis of 14-MeV proton scattering results. The diffraction pattern of the 3.16-MeV level seen in this experiment is not very pronounced, but the phase with respect to the elastic scattering angular distribution appears to be consistent only with an odd-l, single-phonon excitation. The small angle behavior of the angular distribution is only consistent with a plus parity assignment. A 1^+ or 3^+ state would have to go by a magnetic transition in an electron scattering process and thus it would not be expected to be excited strongly at forward angles. Since it is strongly excited in inelastic electron scattering at forward angles the most likely remaining assignment is two-phonon 4^+ state. The best DWBA fit to the proton data was for $l=2$. Thus we have shown 2^+ for the state in Table III. However, the present DWBA code cannot do calculations for two phonon states.

G. Ni^{58}

Excited states of Ni^{58} have been observed at $1.45(2^+)$, 3.33, and 4.5 MeV (3^-) (Fig. 8). Angular distributions have been taken for the 1.55- and 4.45-MeV states (Fig. 16). Broek *et al.*[8] have observed states of Ni^{58} at 1.45, 2.47, 3.3, 4.45, 5.5, 5.9, 6.8, and 7.1 MeV. Crannel *et al.*[4] observed states at 1.45, 2.5, 3.2, 3.5, 4.5, and 7.55 MeV. Our data, the alpha-particle data, and the electron data are consistent with assignments of 2^+ to the 1.5-MeV state and 3^- to the 4.5-MeV state.

Figures 19 through 21 contain Blair-Drozdov and PWBA fits to the elastic and inelastic proton scattering for Ni^{58}.

The DWBA fit to the Ni^{58} elastic and inelastic data is given in Fig. 24. The extracted G values are 12.5 and 12.9 for the $Q=-1.45$-MeV 2^+ state and the $Q=-4.5$-MeV 3^- state, respectively. These G values are in good agreement with the values of 14 and 13 obtained from inelastic electron scattering[4] for the same states and the value of 11.8 for the 2^+ state measured by Coulomb excitation.[33] The DWBA fit to the elastic scattering is excellent, and the inelastic fits are good.

G values have been extracted from a DWBA analysis of the alpha scattering[22] from Ni^{58} yield G values of 10.2 for the $Q=-1.45$, 2^+ state which is in fair agreement with the values extracted from proton and electron scattering from Ni^{58}. The value obtained for the 3^- state, $Q=4.5$ MeV, is 6.3 which is a factor of two lower than the proton and electron values. The G's derived from the Blair-Drozdov theory for the alpha data do not agree with the DWBA values. The situation is the same when comparing Blair DWBA values of G for the proton data. This can be attributed to the arbitrariness in the normalization of the data to the comparatively poor Blair-Drozdov fits.

H. Ni^{60}

States of Ni^{60} have been observed at 1.36, 2.55, 3.23, 4.05, 5.13, and 7.08 MeV (Fig. 9). Angular distributions have been measured for levels at 1.36, 2.55, 4.05, and 5.13 MeV (Fig. 17). Broek *et al.*[8] in high-resolution inelastic alpha scattering have observed levels in Ni^{60} at 1.33, 2.2, 2.5, 3.2, 4.05, 5.1, 5.6, 6.2, and 7.0 MeV. Using 183-MeV electrons Crannel *et al.*[4] have observed strong levels at 1.33, 2.50, 4.05, and 5.1 MeV. For the three bombarding particles one finds that the same states are excited with about the same relative probability. Crannel *et al.* assign for the spins and parities of the 1.33-MeV level, 2^+; for the 2.5 level, 4^+; for the 4.05-MeV level, 3^-; and for the 5.1-MeV level, 4^+; both our work (for the 1.36- and 4.05-MeV states) and the alpha-particle work is consistent with these assignments.

DWBA fits to the elastic scattering and the inelastic scattering for the $Q=-1.33$-MeV and $Q=-4.05$-MeV state are shown in Fig. 25. G values deduced for the states are given in Table III. The G values for the $Q=-1.33$-MeV 2^+ state of 16.6 is in excellent agreement with the value of 16 obtained via Coulomb excitation[33] and the value 17 obtained from inelastic electron scattering measurements.[4] The G values obtained from inelastic proton scattering for the remaining levels are in fair agreement with those obtained from inelastic electron scattering, especially considering our large errors for the 2.55- and 5.13-MeV states.

[33] D. S. Andreyov, A. P. Grinberg, K. I. Erökhina, and I. Kh. Lenberg, Nucl. Phys. **19**, 400 (1960).

I. Pb^{208}

States of Pb^{208} were observed at 2.62, 4.35, 5.66, and 7.40 MeV (Fig. 10). Crannel *et al.*[4] have observed states at 2.6 and 4.3 MeV.

The angular distribution of protons inelastically scattered from the 3^-, 2.6-MeV level of Pb^{208} is shown in Fig. 18. The G value from the DWBA analysis (Fig. 26) is given in Table III. The value found by us using the DWBA fit is in fair agreement with the value determined by inelastic electron scattering. The Blair theory however gives a very poor value, but again, the Blair normalization is very arbitrary.

V. CONCLUSIONS

The PWBA and Blair-Drozdov theories give very poor fits to the inelastic proton angular distributions. The predicted angular distributions have minima which are too deep and a fall-off with angle which is much less than is observed. It is found that the Blair phase rule is satisfied only moderately well for inelastic proton scattering at 40 MeV for those states which show a diffraction structure.

The data support the ideas of Kromminga and McCarthy concerning the small angle behavior of the differential inelastic scattering cross section. In all cases where angular distributions were obtained in the experiments, the parity assignments from the small angle scattering were consistent with assignment from other sources except for inelastic scattering from the 3.16-MeV state of Fe^{56}. Our parity assignment agrees with the assignment from other proton work[1] but disagrees with assignment deduced from inelastic electron[4] and alpha scattering.[6]

The optical model DWBA give excellent fits to the elastic scattering and good fits to the inelastic scattering.

The G values obtained from electron scattering and other electromagnetic processes, and those obtained from Satchler and Fricke's collective DWBA analyses of inelastic proton scattering generally are in good agreement although there are several discrepancies of a factor of two. With more accurate data and further refinement of the DWBA analysis, accurate $B(EL)$ values can probably be obtained for many states from inelastic proton scattering data.

ACKNOWLEDGMENTS

The authors are indebted to Dr. L. L. Lee, Jr., who supervised the early phases of this experiment. We would also like to express thanks to Martin P. Fricke and Dr. G. R. Satchler for supplying the DWBA calculations and allowing us to publish their work. Thanks must be given to Dr. J. H. Williams for his interest in the experiment. Appreciation is extended to Dr. Neville Reay, and Dr. Charles Kavaloski for helping with the data collection.